Extended scenarios for solar radio emissions with downshifted electron beam plasma excitations

M. Lazar[1,2], R. A. López[3,4], S.M. Shaaban[5], S.Poedts[1,6], H. Fichtner[7]

[1]Centre for Mathematical Plasma Astrophysics, KU Leuven, Celestijnenlaan 200B, B-3001 Leuven, Belgium
[2]Institut für Theoretische Physik IV, Ruhr-Universität Bochum, D-44780 Bochum, Germany
[3] Research Center in the intersection of Plasma Physics, Matter, and Complexity (P^2mc), Comisión Chilena de Energía Nuclear, Casilla 188-D, Santiago, Chile
[4]Departamento de Ciencias Físicas, Facultad de Ciencias Exactas, Universidad Andres Bello, Sazié 2212, Santiago 8370136, Chile
[5]Department of Physics and Materials Sciences, College of Arts and Sciences, Qatar University, 2713 Doha, Qatar
[6]Institute of Physics, University of Maria Curie-Skłodowska, ul. Marii Curie-Skłodowskiej 1, 20-031 Lublin, Poland
[7]Institut für Theoretische Physik IV, Ruhr-Universität Bochum, D-44780 Bochum, Germany

Key Points:

- Denser or colder electron beams than in the standard plasma emission model generate downshifted excitations, observed in terrestrial foreshock.
- Kinetic theory and simulations suggest direct and indirect involvement of downshifted excitations in the generation of radio emissions.
- The downshifted excitations are involved directly in the generation of the second radio harmonic, very effectively for systems with two electron counter-beams.

Corresponding author: S.M.Shaaban, shamd@qu.edu.qa; s.m.shaaban88@gmail.com

Abstract

First-principle studies of radiative processes aimed at explaining the origin of type II and type III solar radio bursts raise questions on the implications of downshifted electron beam plasma excitations with frequency (slightly) below the plasma frequency ($\omega \lesssim \omega_{pe}$) in the generation of radio emissions. Unlike the beam-induced Langmuir waves ($\omega \gtrsim \omega_{pe}$) in the standard radio emission plasma model, the primary wave excitations of cooler and/or denser beams have predominantly downshifted frequencies. Broadbands of such downshifted excitations are also confirmed by in situ observations in association with terrestrial foreshock and electron beams (in contrast to narrowband Langmuir waves), but their involvement in radiative processes has not been examined so far. We revisit three radiative scenarios specific to downshifted primary excitations, and the results demonstrate their direct or indirect involvement in plasma radio emission. Downshifted excitations of an electron beam primarily play an indirect role, contributing to the relaxation to a plateau-on-tail still able to induce Langmuir beam waves that satisfy conditions for nonlinear wave-wave interactions leading to free radio waves. At longer time scales, the primary excitations can become predominantly downshifted, and then directly couple with the secondary (backscattered) Langmuir waves to generate the second harmonic of radio emissions. Two counterbeams are more efficient and lead to faster radiative mechanisms, involving counterpropagating downshifted excitations, which couple to each other and generate intense, broadband and isotropic radio spectra of downshifted second harmonics. Such a long-lasting (second) radio harmonic can thus be invoked to distinguish regimes with downshifted ($\omega \gtrsim \omega_{pe}$) primary excitations.

Plain Language Summary

In cosmology, astrophysics, but also in the solar and geophysical contexts, radio emissions are true messengers of their distant sources, whose interpretation is generally based on the standard radio emission model of the electron-beam plasmas exciting Langmuir electrostatic waves. With frequencies higher than the plasma frequency, intense Langmuir waves can directly engage in wave-wave interactions, leading to escaping radio electromagnetic waves. Present analysis strongly suggests that primary excitations with lower frequencies but still close to the plasma frequency may also contribute, directly or indirectly, to the generation of radio emissions. These downshifted excitations are confirmed by the observations, but are produced by denser and/or cooler electron beams than in the standard model, markedly expanding the parametric regimes to be considered in the remote diagnosis of radio sources.

1 Motivation

Radio emissions represent a topic of great interest in space and astrophysical applications, especially for the exploration of plasma sources that are inaccessible to in situ observations (Warmuth & Mann, 2005; Cremades et al., 2015; Crosley et al., 2016; Mann, G. et al., 2018; Villadsen & Hallinan, 2019; Davis et al., 2021). However, indirect remote diagnostics requires an understanding of the physical mechanisms that produce radio emissions and, implicitly, realistic modeling of plasma systems and the physics involved (Nindos et al., 2008; Pick & Vilmer, 2008; Reid & Ratcliffe, 2014). The most cited source of radio emissions are the electron beams released by energetic solar events, relevant being type II radio bursts associated with interplanetary shocks generated by coronal mass ejections (CMEs), but also type III radio bursts triggered by energetic electrons from coronal flares (Lin et al., 1981; Bale et al., 1999; Pulupa & Bale, 2008; Mann, G. et al., 2018). The ability of electron beams to produce radio emissions is predicted by theory (Cairns, 1989; Ziebell et al., 2014; Ziebell et al., 2016; Lazar et al., 2023a), and is ultimately proven by numerical simulations (Kasaba et al., 2001; Rhee et al., 2009; Umeda, 2010; Ganse et al., 2012a; Ganse et al., 2012b; Thurgood & Tsiklauri, 2015; Henri et al., 2019; Sauer et al., 2019; Krafft &

Savoini, 2021, 2022; Lee et al., 2022; Lazar et al., 2023a; Bacchini & Philippov, 2024). The linear (kinetic) theory identifies the primary wave excitations of electron beams (Cairns, 1989; Lazar et al., 2023a), while, for example, a weak turbulence (WT) approach explains their nonlinear wave-wave conversion into radio electromagnetic (EM) waves (Ziebell et al., 2014; Ziebell et al., 2016; Lee et al., 2019). Theory is therefore crucial for the interpretation of PIC simulations as well as the observations. The most invoked are plasma emission mechanisms centered on primary excitations of Langmuir waves (symbolized by L hereafter) with frequencies near and above the plasma frequency, $\omega \gtrsim \omega_{pe}$ (Melrose, 2008). At high intensities, L waves satisfy wave-wave decays, leading to daughter waves, i.e., ion-sound (S) waves and secondary L' waves, $L \rightarrow S + L'$, which will then allow couplings (coalescence) to generate EM or transverse (T) waves via, e.g., $L + S \rightarrow T = F$ for the fundamental emission (F), and $L + L' \rightarrow 2T = H$ for the second order harmonic (H).

The primary excitations are, however, highly dependent on the properties of the electron beams, such as their density, bulk velocity or drift relative to the bulk or core population, thermal and suprathermal spread, and, nevertheless, the beam configuration, as either a singular beam aligned to an open magnetic field or two counter-beams (bi-directional electrons) in, e.g., a closed magnetic field topology. On the one hand, the excitation of L waves is limited to a narrow parametric regime, i.e., electron beams (subscript b) with very low number densities n_b and whose speeds U_b satisfy (Cairns, 1989; Gary, 1993)

$$\theta_b < U_b < (n_e/n_b)^{1/3}\theta_b, \tag{1}$$

where $\theta_b = (2\pi k_B T_b/m_e)^{1/2}$ is the thermal spread (or velocity) and T_b the temperature of beam population, m_e is the electron mass and n_e the total number density of electrons. On the other hand, for certain setups in PIC simulations of radio emissions, the electron beams trigger in the preliminary phase instabilities of electron beam (EB) modes, with downshifted frequencies slightly below the plasma frequency, $\omega \lesssim \omega_{pe}$ (Sauer et al., 2019; Lazar et al., 2023a). In this case, we deal with cooler and/or denser beams, which generally satisfy

$$U_b > (n_e/n_b)^{1/3}\theta_b, \tag{2}$$

and excite yet resonant electrostatic (ES) waves from the branch of the electron-beam mode with (an almost) linear wavenumber (k) dispersion of the wave frequency (ω), $\omega \simeq kU_b$. Moreover, these setups still comply with observational estimations for the magnetized electron-beam plasma parameters in the source regions of solar radio bursts. Therefore, such results raise questions about downshifted waves as primary excitations, if they are involved, and if so, in what processes they are involved in producing radio emissions. Because downshifted EB waves contrast with the primary excitations in the standard model of plasma radio emission, which are generally assimilated to L-type waves with a sufficiently high frequency $\omega \gtrsim \omega_{pe}$. Unlike L waves, downshifted waves (with $\omega \lesssim \omega_{pe}$) cannot undergo wave-wave decays specific to standard plasma emission, failing to satisfy the Manley-Rowe laws of conservation for energy and momentum.

The ES plasma oscillations with downshifted frequencies are observed in the terrestrial foreshock or upstream regions in association with electron beams as broadband fluctuations that contrast strongly with narrowband L waves (Fuselier et al., 1985; Onsager & Holzworth, 1990; Soucek et al., 2019). To our knowledge, there are no similar in situ observations of interplanetary foreshocks, but the analyses of bursty radio emissions from the Earth foreshock (Lacombe et al., 1988; Reiner et al., 1997; Kasaba et al., 2000) in conjunction with in situ observations strongly suggest that the underlying physics of electron beams and induced waves is common to all planetary and interplanetary foreshocks, including type II radio burst sources (Boshuizen et al., 2004; Kuncic & Cairns, 2005). Moreover, the parameters of electron beams associated with downshifted ES excitations (Soucek et al., 2019) appear to be similar to the sources of type II radio emission (Pulupa & Bale, 2008), as also noted by (Lazar et al., 2023a).

Early theories and numerical simulations also support generation of downshifted waves, although the (initial) beams are often assumed to be much cooler than the core population,

Table 1. Electron and proton plasma parameterization for the three cases investigated here. Two electron configurations are distinguished: core-beam (C-B) in cases 1 and 2 and core-counterbeams (C-CBs) in case 3. The EB instability is also characterized by the maximum growth rate (γ_m/ω_{pe}) and the corresponding frequency (ω_m/ω_{pe}) and wave number ($\theta_e k_m/\omega_{pe}$) obtained from linear theory (Lazar et al., 2023a).

Parameters \ Cases	1 (C-B)	2 (C-B)	3 (C-CBs)
$T_e = T_c = T_b$ (10^6 K)	2.32	2.32	2.32
$\theta_e = \theta_c = \theta_b$ (10^6 m/s)	8.4	8.4	8.4
$T_p = 0.73\,T_e$ (10^6 K)	1.70	1.70	1.70
$N_b = n_b/n_e$	0.0057	0.05	0.05
U_b/θ_e	16	8	8
γ_m/ω_{pe}	0.104	0.196	0.195
ω_m/ω_{pe}	0.951	0.897	0.877
$\theta k_m/\omega_{pe}$	0.066	0.142	0.139

with, i.e., peak-on-tail rather than bump-on-tail distributions (presumably closer to the source of beam injection than the more relaxed states observed in situ) (Fuselier et al., 1985; Onsager & Holzworth, 1990; Dum, 1990a, 1990b). The simulations generally confirm a transition from reactive or weakly resonant beam modes, with frequencies below plasma frequency ω_{pe}, to the kinetic instability of Langmuir-beam (LB) waves with $\omega \sim \omega_{pe}$, corresponding to the beam relaxation to a more gentle bump-on-tail and even a flattened plateau-on-tail distribution (Dum, 1990a, 1990b; Thurgood & Tsiklauri, 2015; Sauer et al., 2019). Under the wave-particle interaction, the beam slows down and widens at the same time, and the velocity distributions depart significantly from the Maxwellian beam-plasma components assumed initially. The kinetic regime seems to be more robust, lasting much longer than the broadband reactive regime, and downshifted excitations with frequency below but still near plasma frequency ($\omega \lesssim \omega_{pe}$) persist for a long time until the bump in the electron distribution is completely flattened (Dum, 1990a, 1990b). These profiles resemble those from the evolution of gentle beams or marginally stable (plateaued) distributions, which are also associated with periods of local L excitations during solar type III radio bursts (Ergun et al., 1998).

For hot beams, with temperatures similar to that of the core population[1], the excitation of downshifted electron beam (EB) modes implies much higher relative drifts or beam speeds (Sauer & Sydora, 2012; Soucek et al., 2019; Sauer et al., 2019; López et al., 2020; Lazar et al., 2023a, 2023b). Although primary excitations can also be EB modes with (slightly) downshifted frequencies, $\omega \lesssim \omega_{pe}$, emphasis was placed on LB excitations with frequencies $\omega \gtrsim \omega_{pe}$ triggered by the subsequent, more relaxed (plateaued) distribution (Thurgood & Tsiklauri, 2015; Sauer et al., 2019). The later emerges from the standard dispersion curve for L waves ($\omega^2 = \omega_{pe}^2 + 3k^2\theta_e^2$) in a plasma without a beam component (Baumgärtel, 2014; Thurgood & Tsiklauri, 2015). For sufficiently dense or/and cool beams, as our setups in Table 1, the L dispersion curve in the (forward) direction of the beam (i.e., $k_\parallel > 0$), breaks into two branches (Cairns, 1989). One is the LB branch (also known as the electron-acoustic branch) at large $k > \omega_{pe}/U_b$, and the other in the optical domain (small k) couples to the linear dispersion of the EB modes $\omega \simeq k(U_b + \theta_e)$, which increases steeply (above ω_{pe}) with k. The high frequency waves from the LB branch are roughly described by

[1] Hotter or suprathermalized beams/strahls with $U_b \leqslant \theta$, are typical to the solar wind (in the absence of energetic events), and are rather susceptible to EM or hybrid excitations, known as firehose and whistler heat-flux instabilities (López et al., 2020).

$(\omega - kU_b)^2 \simeq \omega_{pe}^2 + k^2\theta^2$ (Swanson, 2003), and are not destabilized by the electron beam. These two branches depart from each other for denser or/and cooler beams. Only very weak beams, with very low densities, e.g., $n_b/n_e < 0.005$, can destabilize L or LB waves, because their dispersion curve ($\omega^2 \simeq \omega_{pe}^2 + 3k^2\theta_e^2$) does not break, but only undulates near unstable wavenumbers (Cairns, 1989; Lazar et al., 2023b). In the backward direction ($k_\parallel < 0$), the L mode is not affected by the beam, but is still distinguishable in the quasithermal fluctuations and the parametric (secondary) excitations. At oblique propagation and large k, both the LB (forward) and L (backward) dispersion curves merge with the Z-mode, becoming what is called the Langmuir/Z (LZ) mode (Benson et al., 2006). In contrast to downshifted EB excitations, L and LB waves are, indeed, typical of the plasma emission model, which includes nonlinear decay $L \to S + L'$ into secondary L' oscillations with low wavenumber $k_{L'} \to 0$, and S waves with $k_S \sim k_L$. Further nonlinear couplings can produce transverse radio waves, both fundamental and harmonic emissions (see above). Moreover, long-lived (or free-damping) L waves of low wavenumbers ($k_L c \sim \omega_{pe}$) can couple and linearly convert to EM radio waves with oblique propagation (Sauer et al., 2019). This process can last longer until the plateau relaxes, which provides a plausible explanation for Sturrock's dilemma (Sturrock, 1964).

In the present paper, we build on such results in, for instance, Sauer et al. (2019) and Lazar et al. (2023a), seeking to clarify the role of downshifted plasma excitations in radio wave production. We have refined and extended particle-in-cell (PIC) simulations for the three cases in Lazar et al. (2023a), to examine configurations with a single (asymmetric) electron beam and also two symmetric counterbeams (see Table 1), involving distinct radiative processes. Electron counterbeams typically produce radio harmonics on shorter time scales and with higher intensities (Umeda, 2010; Ganse et al., 2012b), in this case, broadband second harmonics with downshifted frequencies, see also Lazar et al. (2023a). However, none of the previous studies investigated the involvement of downshifted excitations, neither primary excitations nor radio EM waves. Studies of radio emissions often assume similar or even identical parameterizations of electron beam plasmas, but mostly in the absence of an ambient magnetic field and without reference to downshifted excitations (Baumgärtel, 2014; Thurgood & Tsiklauri, 2015; Henri et al., 2019). The influence of the magnetic field (B_0) was also examined in PIC simulations, for strong fields or underdense plasmas with $\omega_{pe} \leqslant |\Omega_e|$, where Ω_e is the electron gyrofrequency, and for weakly magnetized or overdense plasmas with $\omega_{pe} > |\Omega_e|$ (Ganse et al., 2014; Sauer et al., 2019; Lee et al., 2022). Radiative processes involving linear and nonlinear wave interactions remain the same in nature, and only the spectra of primary and radio wave excitations undergo changes. Here, we provide a plausible explanation for the enhancement of the second radio harmonic in the presence of the magnetic field (Lee et al., 2022).

We use an explicit 2D PIC code based on the KEMPO1 code of Matsumoto and Omura (1993). The basic setup in the simulations consists of the following: a spatial domain composed of 1024×1024 grid points, with $\Delta x = \Delta y = 0.04\, c/\omega_{pe}$ and 625 particles per species per cell, and a time-step $\Delta t = 0.01/\omega_{pe}$, a realistic mass ratio $m_p/m_e = 1836$, and both the core and beam populations implemented as drifting Maxwellians (since the shape of the velocity distribution is not of interest in our analysis)[2]. We assume moderate magnetic field intensities, i.e., $\omega_{pe}/|\Omega_e| = 100$, as in Kasaba et al. (2001); Rhee et al. (2009) and Lazar et al. (2023a), and also consistent with data linked to plasma sources of solar radio emissions (Ergun et al., 1998; Bale et al., 1999; Pulupa et al., 2010).

[2] In the solar wind, suprathermal tails of Kappa distributions (Pierrard & Lazar, 2010) reduce the beam-core anisotropy, inhibit the electron-beam instability, and can even switch to the unstable regime of L or LB modes (Lazar et al., 2023b). This explains why radio emissions require higher beam speeds to compensate for the effects of suprathermal electrons (Li & Cairns, 2013, 2014).

2 Cases of interest

We reconsider the three electron beam plasma configurations in Lazar et al. (2023a), all leading to primary waves with upshifted but mainly downshifted frequencies: two configurations with a single beam of electrons and one with counter-beams, whose parameters are summarized in Table 1.

2.1 Case 1

We first refer to PIC simulations of plasma emissions involving a single electron beam and start with case 1 in Table 1. The upper panels in Figures 1–3 display (normalized) wave energy density computed as spatio-temporal Fast Fourier Transforms (FFTs) of the parallel electric field component, $|\mathrm{FFT}(\delta E_\parallel/B_0)|^2$. The wave dispersion curves derived (for initial conditions) from linear theory (Cairns, 1989; Lazar et al., 2023a) are also shown: the L waves, with the forward ($k > 0$) L_+ branch and the backward ($k < 0$) L_- branch, with white dashed lines; the almost linear branch of EB waves at low k, continued after the shoulder (at $\sim \omega_{pe}$) with the LB branch at higher k, with red dashed lines; and for reference, the white dotted line indicates $\omega = \omega_{pe}$. For the initial condition in case 1, theory predicts an instability of EB modes with maximum growth rate (Table 1) corresponding to a slightly downshifted (normalized) frequency $\omega_m/\omega_{pe} = 0.951 \lesssim 1$ and a (normalized) wavenumber $\theta_e k_m/\omega_{pe} = 0.006$ (Lazar et al., 2023a). In numerical simulations, as well as in real plasma systems, in addition to this fastest-growing mode, all neighboring modes with finite growth rates are subsequently excited. The primary excitations actually have a spectrum of finite widths in frequency and wavenumber, around the fastest-growing EB mode. The primary wave excitations are therefore found in a band of lower or higher frequencies, which means that the primary spectra contain both downshifted and upshifted frequencies.

The simulated spectra show the transition along the red-dashed dispersion curve in Figure 1, from the primary excitations, predominantly EB modes, to LB excitations[3] (Sauer et al., 2019; López et al., 2020). From left to right panels, we find a transition from $\omega/\omega_{pe} \lesssim 1$ and low wavenumbers $\theta_e k/\omega_{pe} \lesssim 0.1$, to LB waves at $\omega/\omega_{pe} \gtrsim 1$ and larger wavenumbers $\theta_e k/\omega_{pe} \gtrsim 0.1$. Correspondingly, the wave spectra in Figure 2, upper panels, show maximum intensities evolving toward larger (parallel) wavenumbers, compared to the dashed line marking the initial maximum. These spectra are plotted as a function of parallel and perpendicular wavenumbers by averaging the spectra in Figure 1 around the plasma frequency, specifically over the interval $0.8 < \omega/\omega_{pe} < 1.2$. For $\omega_{pe}t > 300$, these high-frequency spectra are dominated by LB excitations, as the culminating stage of the transition from downshifted to upshifted excitations. Higher harmonics of LB waves are also excited at $\sim 2\omega_{pe}$ and $\sim 3\omega_{pe}$ (Gaelzer et al., 2002; Yoon et al., 2003; Sauer & Sydora, 2012), with higher intensities in the forward direction. Upshifted LB waves conform to the standard plasma model of radio emission and can engage in wave-wave interactions (with, e.g., S and L waves) to ultimately produce T radio waves (Melrose, 2008), as explained in Section 1.

The spectra of (normalized) magnetic wave energy density, computed as $|\mathrm{FFT}(\delta B_\perp/B_0)|^2$, are displayed in Figure 1, lower panel, and Figure 2, middle and bottom panels. In the middle panels, we tracked the F $\rightarrow T$ component, averaging the spectra in the interval $0.8 < \omega/\omega_{pe} < 1.2$, and in the bottom panels the H $\rightarrow 2T$ component in the interval $1.8 < \omega/\omega_{pe} < 2.2$. More intense T wave spectra are also obtained here after $\omega_{pe}t = 300$, both the fundamental (F) and higher (H) harmonics with peak intensities for oblique propagation, and in agreement with the arguments from Sauer and Sydora (2012) and Sauer et al. (2019). Moreover, the evolutions of the electron velocity distributions shown by Thurgood and Tsiklauri (2015) and Sauer et al. (2019) for similar (initial) setups suggest that primary excitations have an indirect, rather than a direct, involvement in the radiative

[3] Also known as electron-acoustic modes, which are however rapidly damped in the absence of a high temperature contrast between the electron populations (Sauer et al., 2019).

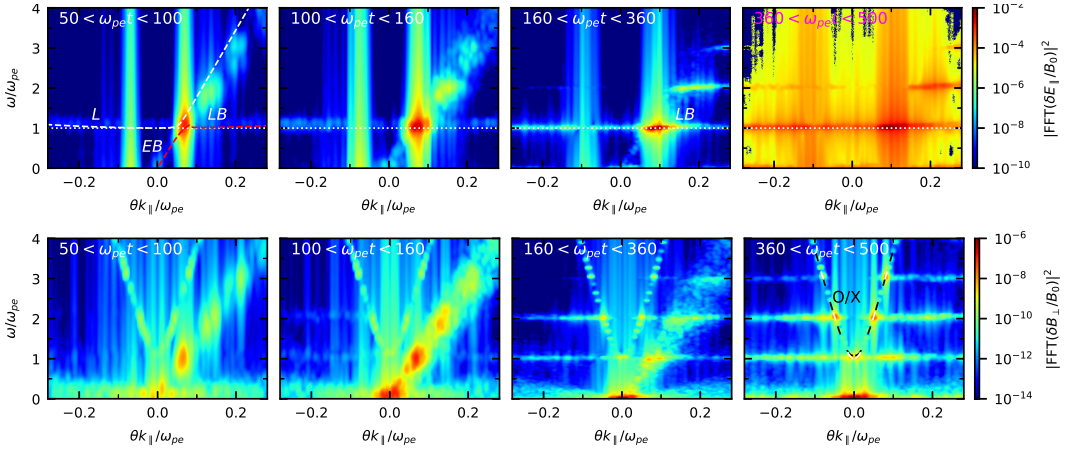

Figure 1. Case 1: Wave energy density spectra (normalized) computed with spatio-temporal FFTs of the parallel electric field (upper) and perpendicular magnetic field (lower) components, as functions of frequency and parallel wavenumber, for different temporal intervals at $k_\perp = 0$.

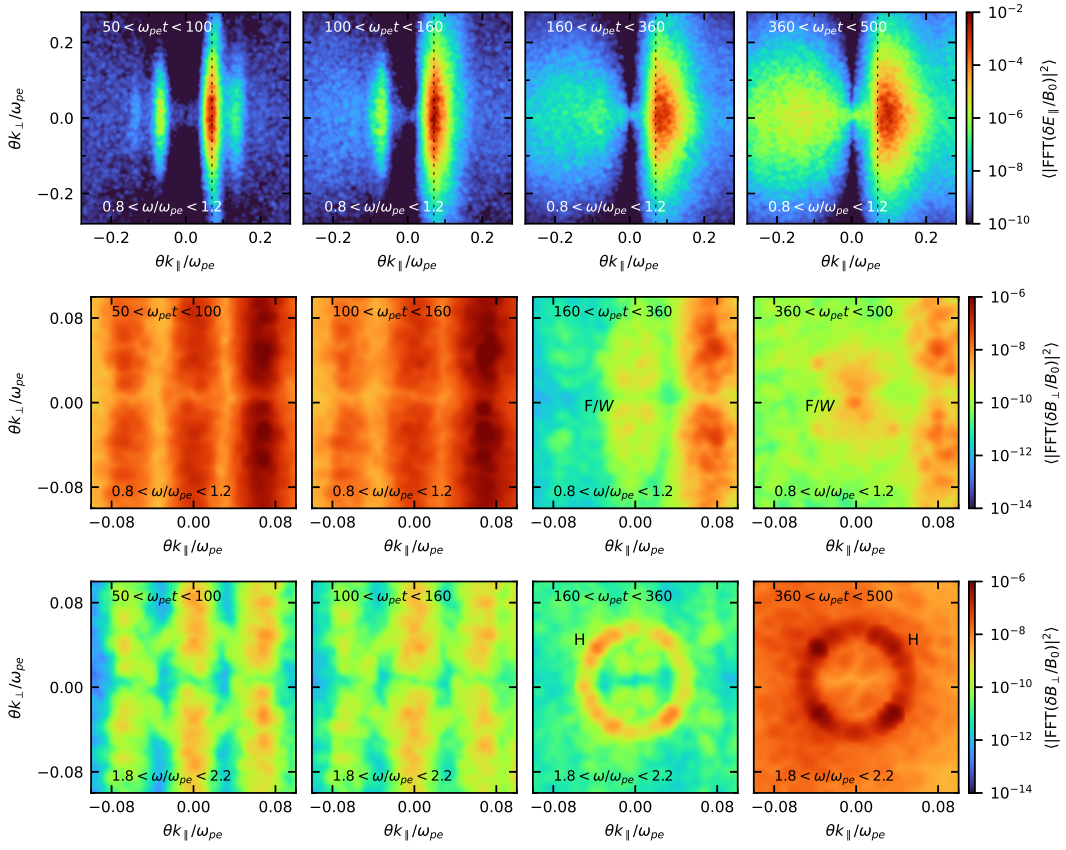

Figure 2. The same wave energy density spectra (normalized) as in Figure 1, but as functions of parallel and perpendicular wavenumbers (normalized), and averaged in the frequency intervals $0.8 < \omega/\omega_{pe} < 1.2$ (top and middle panels), and $1.8 < \omega/\omega_{pe} < 2.2$ (bottom panels).

process. Specifically, growing fluctuations are effective in relaxing and flattening the beam, as proved both in the absence (Thurgood & Tsiklauri, 2015; Henri et al., 2019; Lee et al.,

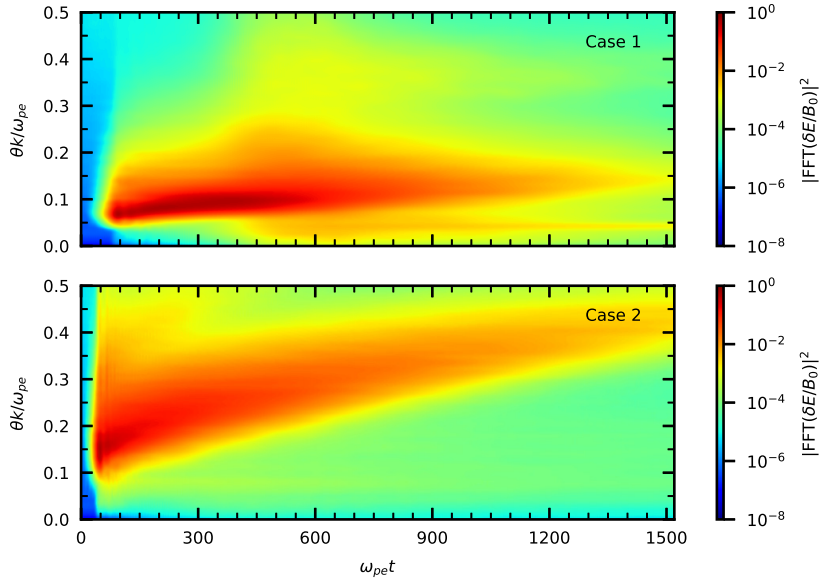

Figure 3. Temporal evolution of $|\mathrm{FFT}(\delta E/B_0)|^2$ for case 1 (upper) and case 2 (lower), each of them color-coded and as a function of total wavenumber $k = (k_\parallel^2 + k_\perp^2)^{1/2}$.

2019) and in the presence of a magnetic field (Kasaba et al., 2001; Sauer et al., 2019; Lee et al., 2022). Such that the beam relaxes to a plateau-on-tail distribution of lower density but hotter, which can trigger L or LB waves with higher frequencies, predominantly above the plasma frequency, $\omega \geqslant \omega_{pe}$. LB waves with large enough k can decay into forward propagating S waves and L waves with low-k (optical range), $LB \rightarrow L + S$, a wave-wave decay also known as Langmuir condensation (Lee et al., 2019).

In addition, Sauer et al. (2019) invoked a mechanism distinct from those in the standard plasma model, namely, linear mode conversion (LMC) of low-k L waves to T waves. Originally predicted for non-magnetized plasmas, when coupling of longitudinal L waves and radio T waves is facilitated by the presence of inhomogeneities (Field, 1956), LMC is also invoked for type II and type III bursts (Lin et al., 1981; Melrose et al., 1985; Cairns, 2011), and in planetary magnetospheres (Yoon et al., 1998; Menietti et al., 2009; Schleyer et al., 2014). LMC operates when dispersion curves, wave frequency vs. wavenumber (ω vs. k), approach or even cross each other (Sauer et al., 2019). In overdense plasmas ($\omega_{pe} > |\Omega_e|$), the dispersion curves of the L mode and the free EM modes, left-handed (LH) and right-handed (RH) modes, cross each other for parallel propagation, but their fields remain uncoupled. Instead, oblique modes can couple, that is, Langmuir/Z (LZ) mode with, respectively, the ordinary (O) and extraordinary (X) modes (corresponding to the LH and RH modes in the parallel direction), and their dispersion curves indeed split, proving conversion from one mode to another around the crossing point; see Figure 9 in Sauer et al. (2019). The initial plasma is homogeneous, but if density gradients are generated later in the simulation, the parallel L modes may also undergo LMC into radio emissions (Field, 1956; Volokitin & Krafft, 2020). For parallel propagation in Figure 1 (last lower panel), the O and X modes are also indicated with dashed lines, white and black, respectively. In overdense plasmas these two modes overlap, and only near ω_{pe} the O mode is slightly downshifted (Lee et al., 2022), which can explain the observed F emission (as an O mode) with a weak partial polarization and an almost depolarized second H component (Raja & Ramesh, 2013; Pulupa et al., 2020).

In our Figures 1 and 2, the spectra in the fourth upper panels are consistent with both scenarios, showing excitations of LB and L waves at $\sim \omega_{pe}$, but also S waves at much lower frequencies, along a wide range of wavenumbers, including both forward and backward propagation. Also, the 2D spectra in the last two upper panels of Figure 2 confirm the extension of the L modes, including the oblique ones, towards the lower $k_{\parallel}$. It is very likely that such bursty spectra of excitations LB, L and S lead to multiple mechanisms capable of producing radio emissions, as discussed below. The upper panel of Figure 3 shows the full evolution of the wave energy density, that is, $|\mathrm{FFT}(\delta E/B_0)|^2$ as a function of the total wavenumber, from our long-run simulation ($\omega_{pe}t_{\max} = 1500$). The transition from low-k excitations (EB modes) to those with larger k (LB waves) starts early, before $\omega_{pe}t = 200$, and after $\omega_{pe}t = 350$ intense primary LB waves occur at even larger k. After $\omega_{pe}t \simeq 400$, clear signatures of the decay of LB waves into daughter waves of higher and lower wavenumbers (S waves and L waves, respectively) are observed, with the branch of the latter distinctly separating at very low $k \to 0$.

The spectra of T-modes in Figures 1 and 2, lower panels, are complex. Free radio waves can escape and propagate in the ambient plasma with sufficiently isotropic spectra, and can thus be identified within circular shapes (Lee et al., 2019, 2022), such as the intense second H emission in Figure 2, lower panels. A typical quadrupole pattern (oblique peaks) of F emission at plasma frequency ($\sim \omega_{pe}$) and low k generally connects with the peaks of H emissions at larger k. The circular shapes of their maxima are more specific to weakly or nonmagnetized plasmas (Lee et al., 2022). Again, our spectra in Figure 1, lower panels, suggest that harmonics of the LB/L-modes undergo LMC into the corresponding radio H waves, where their dispersion curves cross each other, at, e.g., $2\omega_{pe}$, $3\omega_{pe}$, etc. In addition, the 2D spectra in Figure 2, the last two lower panels, confirm the oblique propagation maxima for the radio components F and H. However, given the bursty spectra of primary and parametric excitations in, e.g., Figure 1, last upper panel, not only one but several distinct mechanisms are expected to be at the origin of radio emissions: wave-wave decays, e.g., $LB \to S + T$, and coalescence, e.g., $L_- + S_+ \to T$, $LB + L_- \to 2T$, etc. (where subscripts + and − indicate forward and backward propagation, respectively), but also the LMC discussed above. The high intensity of the excitations corresponding to these modes (but also of the quasi-thermal noise in between) proves that the resonance conditions are fully satisfied, not only between the electron beam and the primary excitations, but also in the wave-wave interactions generating the secondary excitations. In the magnetic wave energy spectra (out-of-plane component, $B_\perp$), lower panels of Figures 1 and 2, we can also recognize the EM electron beam modes excited in the early stage by the Weibel or filamentation-like instability (Lazar et al., 2010), with highly oblique or nearly perpendicular propagation (Karlický, 2009; Thurgood & Tsiklauri, 2015). The radio waves apparently emerge later in these spectra, for, e.g., $\omega_{pe}t > 150$, and with maxima for less oblique wave vectors with comparable components, $k_{\parallel} \sim k_\perp$. The radio component F can be difficult to distinguish due to the Weibel (W) modes, the overlap of the two excitations being indicated by F/W (Figure 2).

2.2 Case 2

In cases 2 and 3 we change the (initial) setups of the electron beam plasma, see Table 1, and downshifted primary excitations are involved again. In case 2, we deal with a single beam as in case 1, but denser ($n_b/n_e = 0.05$) and with a lower relative beam speed ($U_b/\theta_e = 8$). The corresponding FFT spectra obtained in case 2 for the wave energy densities are displayed in Figures 4 and 5. These results correspond to the same time interval that was found relevant for the generation of radio waves in case 1. Returning to Figure 3, the lower panel shows the temporal evolution of $|\mathrm{FFT}(\delta E/B_0)|^2$ in case 2, throughout the entire interval of our extended run ($\omega_{pe}t_{\max} = 1500$).

Looking for explanations for the differences between the spectra in cases 1 and 2, we first turn to the predictions of linear theory for the primary excitations; see in Lazar et al. (2023a)

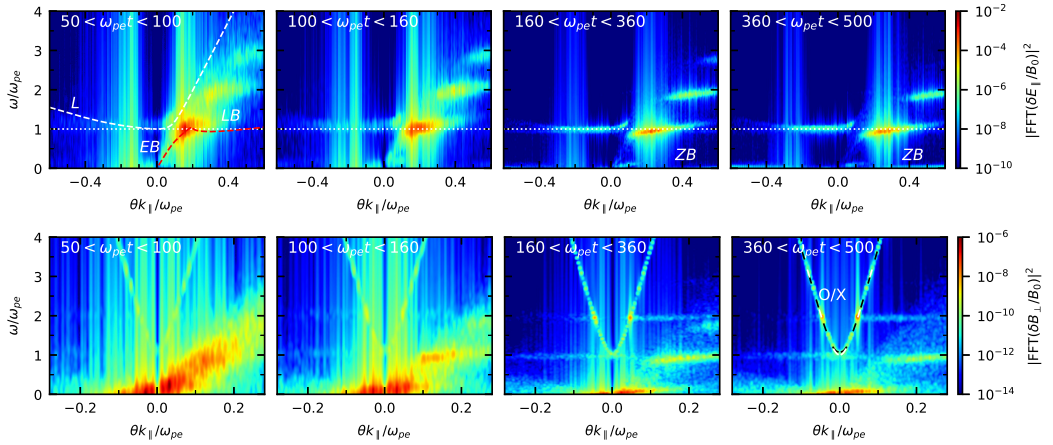

Figure 4. Case 2: Wave energy density spectra (normalized) computed with spatio-temporal FFTs of the parallel electric field (upper) and perpendicular magnetic field (lower) components, as functions of frequency and parallel wavenumber, for different temporal intervals at $k_\perp = 0$.

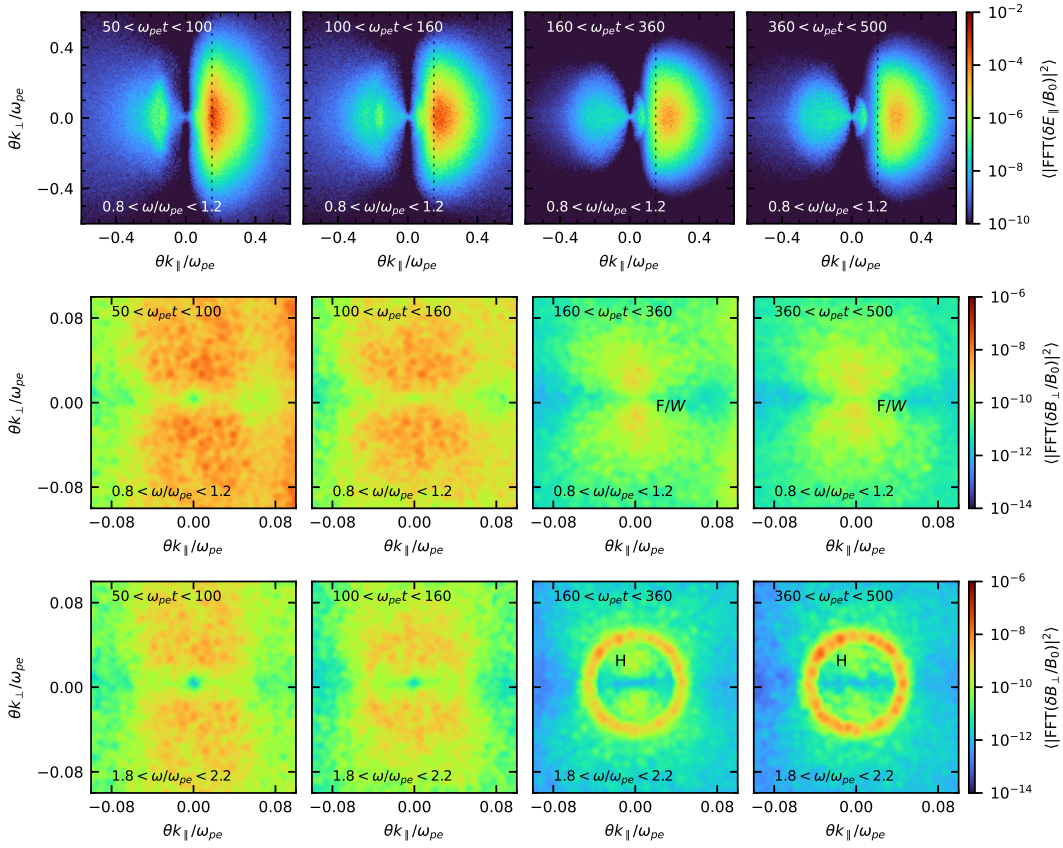

Figure 5. The same wave energy density spectra (normalized) as in Figure 4, but as functions of parallel and perpendicular wavenumbers (normalized), and averaged in the frequency intervals $0.8 < \omega/\omega_{pe} < 1.2$ (top and middle panels), and $1.8 < \omega/\omega_{pe} < 2.2$ (bottom panels).

their Figures 1 and 2, and the related comments. The fastest growing (with maximum growth rate) is also an EB mode with $\omega_{\rm m}/\omega_{pe} = 0.897$, slightly lower than in case 1

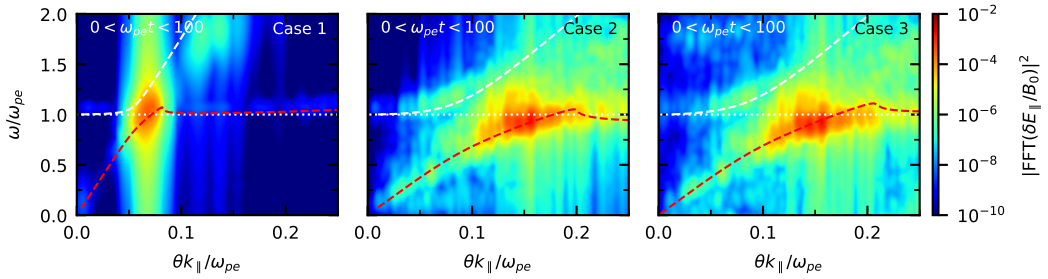

Figure 6. Comparison of the early primary spectra with details of the downshifted excitations.

(Table 1), while the corresponding wavenumber becomes much higher $k_{\rm m}\theta_e/\omega_{pe} = 0.142$ (Lazar et al., 2023a). These values prove that the instabilities of the EB modes ($\omega \simeq kU_b$) are still kinetic or Landau-resonant (as long as their frequency remains close to ω_{pe}). A slightly lower frequency also implies that the early spectrum of primary excitations appears to be more attached to the EB branch and therefore more downshifted along this branch, compared to case 1. This is confirmed by the early spectra of primary excitations compared in Figure 6. In case 2, the primary excitations are more extended along the EB branch, being visibly dominated by the downshifted frequencies below the plasma frequency (ω_{pe}), indicated by the white dotted line.

Initial differences also have consequences later in time when these excitations evolve, also toward larger wavenumbers (upper panels in Figure 5), and contrast to those in case 1; see also the contrast between lower and upper panels in Figure 3. The beam undergoes a similar relaxation to a plateau-on-tail (Thurgood & Tsiklauri, 2015), which again determines the spread of the primary wave maxima along the LB branch (red dashed line) with frequencies predominantly above ω_{pe}, see upper panels of Figures 4 and 5. However, these LB excitations have higher wavenumbers, as also proven by the lower panel in Figure 3, which seems to markedly affect the resonance conditions for the further wave-wave decays. The LB waves have high enough frequencies $\omega \gtrsim \omega_{pe}$, but the lower panel of Figure 3 shows no signature of an effective resonant decay as in case 1. Also, the upper panels of Figure 4, but also those of the subsequent intervals in Figure 7, do not present explosive spectra specific to resonant wave interactions (as in Figure 1, last upper panel). Also, the lower panel of Figure 3 does not show the same prominent decay as in the upper panel in case 1. However, in Figure 4 one can still distinguish parametric (secondary) excitations of much lower intensities, forward propagating S waves with large k and backscattered L_- waves with small k. In turn, the primary and parametric excitations can couple, leading to radio emissions, both the F component, via $L_- + S_+ \to T$, and the second harmonic H, via $LB + L_- \to 2T$. On the other hand, primary LB waves can also decay into a S wave with $k_S \simeq k_L$, and a forward propagating L_+ wave with low k_L in the optical range ($k_L c \sim \omega_{pe}$) via $LB \to S_+ + L_+$. These secondary excitations can be identified in Figure 4, easier to distinguish than in case 1 due to the less bursty and noisy spectra. As discussed in case 1, L waves can be responsible for the generation of T waves of radio F emission through LMC, and if primary LB waves are sufficiently intense, it becomes also possible to decay directly as $LB \to S + T$.

The decay processes of the primary excitations involve a weak wave-wave resonance this time, which makes the intensities reached by the secondary (or parametric) excitations, for example S and L waves, much lower than in case 1. This also affects the processes of coalescence (or coupling) of primary and secondary excitations, and can explain the very low levels of F emission (produced by LMC or a coalescence like $L + S \to T$), barely distinguishable in Figure 4, lower panels, and Figure 5, middle panels (possibly mixed with W excitations). Instead, the second H radio waves remain more prominent, e.g. in the

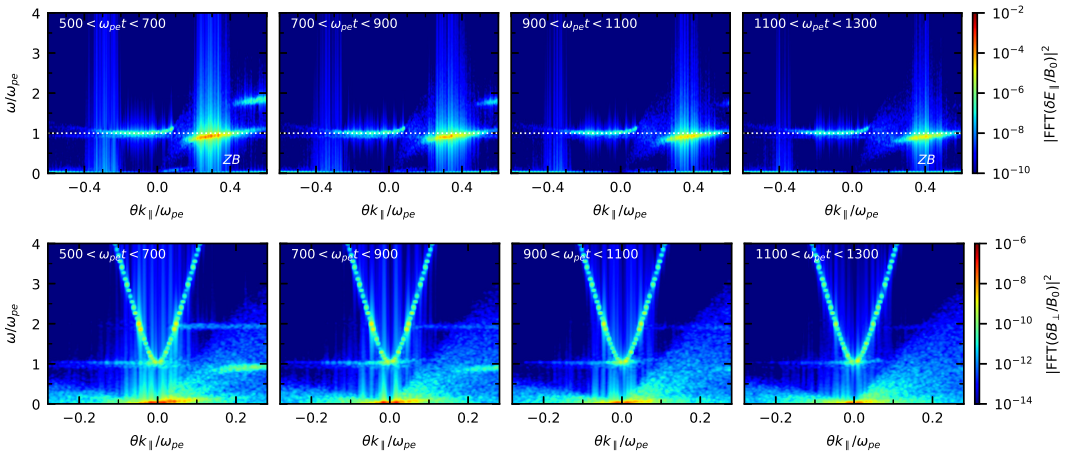

Figure 7. Case 2: The same as in Figure 4, but for extended temporal intervals (indicated in each panel).

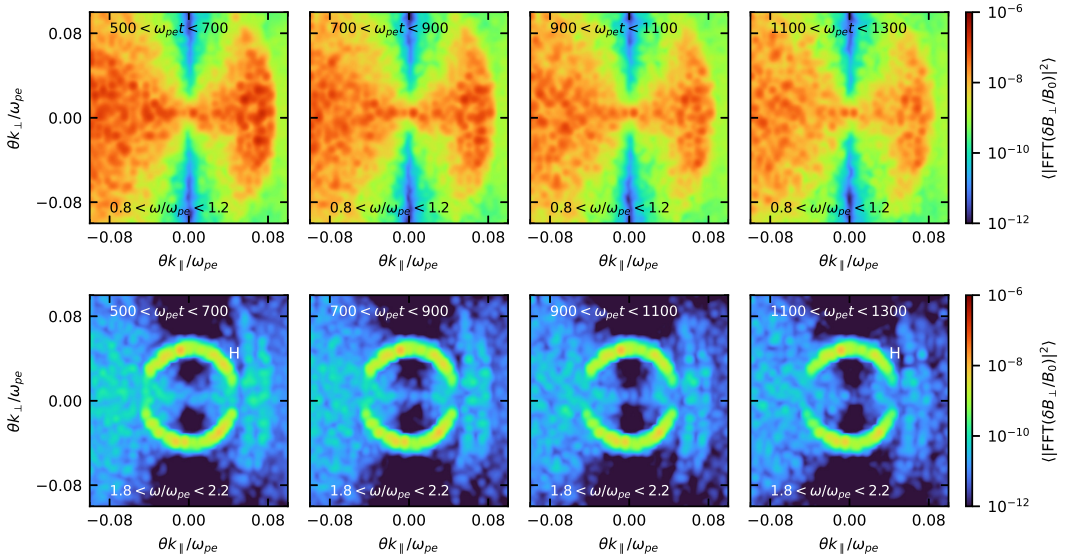

Figure 8. Case 2: The same as middle and bottom panels of Figure 5, but for extended temporal intervals (indicated in each panel).

bottom last panel in Figure 5, even when the primary LB excitations tend to drop below the plasma frequency, in the upper last panel of Figure 4. These modes have frequencies $\omega < \omega_{pe}$ and we call them beam-induced excitations of the Z mode (ZB) (Lee et al., 2022), to distinguish them from LB excitations with $\omega > \omega_{pe}$.

In the longer runs in Figure 7, the primary ZB waves are further attenuated in intensity, and their wide wavenumber band drops below the plasma frequency. Rather, these appear to be electron-acoustic modes excited by a relaxed and thermalized electron beam, as a plateau on the tail, hotter than the core (Sauer et al., 2019). The primary excitations become predominantly downshifted ZB waves (see the upper last panel of Figure 4), while the second H radio emission remains prominent (compared to previous temporal intervals). In addition, the radio emission shows an isotropization tendency, unlike the more quadrupolar

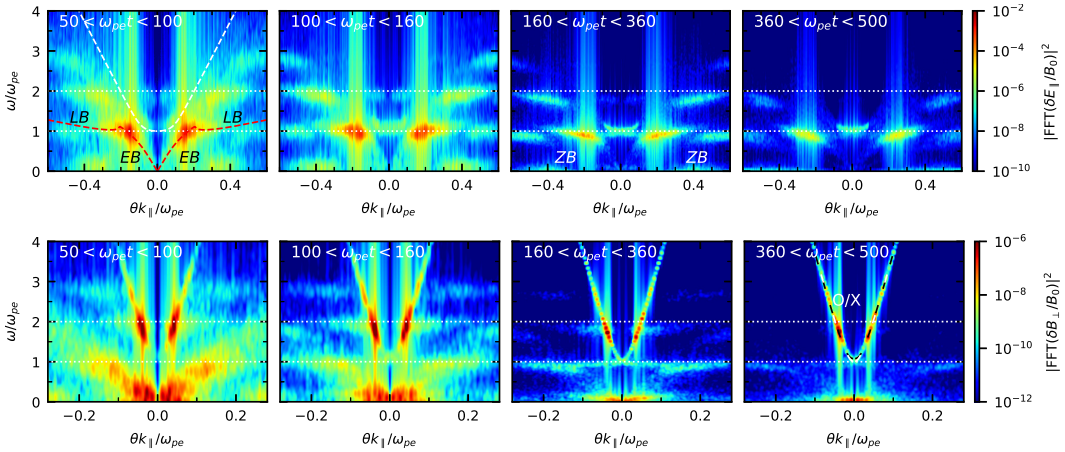

Figure 9. Case 3: Wave energy density spectra (normalized) computed with spatio-temporal FFTs of the parallel electric field (upper) and perpendicular magnetic field (lower) components, as functions of frequency and parallel wavenumber, for different temporal intervals at $k_\perp = 0$.

spectrum in case 1. These features strongly suggest that H emission is the result of the coalescence of primary waves, upshifted LB waves but also downshifted ZB excitations, with parametric L_- modes, namely, via $LB + L_- \rightarrow 2T$ and $ZB + L_- \rightarrow 2T$, respectively. More direct confirmations of the involvement of downshifted ZB primary waves are provided by the spectra of subsequent time intervals in Figures 7 and 8. The upper panels of Figure 7 show fully downshifted ZB-type primary excitations, and correspondingly, a less intense (compared to earlier times) but still appreciable second H radio component is obtained in Figure 8. This is the first concrete evidence for direct involvement of downshifted primary excitations in the generation of radio emissions. In this case, it occurs late (on large time scales) when the beam is already flattened. In case 3 discussed in the following, we will see a faster and more pronounced involvement of the downshifted primary excitations. We cannot rule out that similar processes also take place in case 1 as well, especially during the bursty spectra in the last upper panel of Figure 1, with primary excitations above and below the plasma frequency. In the radio spectra in Figure 2 the emission of the H component is also much more intense than the F component.

2.3 Case 3

In case 3, the plasma system is significantly different, considering two symmetric counterbeams of electrons which lead to major differences in the EM radio wave spectra, as well as in the underlying mechanisms. Double or bidirectional beams, with the same properties as the beam in case 2, see Table 1, produce symmetric spectra of counter-propagating primary excitations (subscripts "+" for forward and "-" for backward propagation), predominantly downshifted with respect to plasma frequency; see also the last panel of Figure 6. The fastest growing modes, both forward and backward propagating, are predicted by linear theory for initial conditions and remain similar to that of case 2, with a slightly lower frequency $\omega_{\rm m}/\omega_{pe} = 0.877$ on the branch EB (red-dashed lines) and a wavenumber $k_{\rm m}\theta_e/\omega_{pe} = 0.139$ (Lazar et al., 2023a).

The simulated spectra of the primary excitations are shown in the upper panels of Figures 9 and 10, for the same time intervals as in Figure 4. In the early phases, that is, $\omega_{pe}t < 160$, both EB modes with downshifted frequencies ($\omega \lesssim \omega_{pe}$) and LB waves with upshifted frequencies ($\omega \lesssim \omega_{pe}$) are excited. The lower panels in Figure 9 and the middle and bottom panels in Figure 10 prove very fast radio generation, most likely triggered by

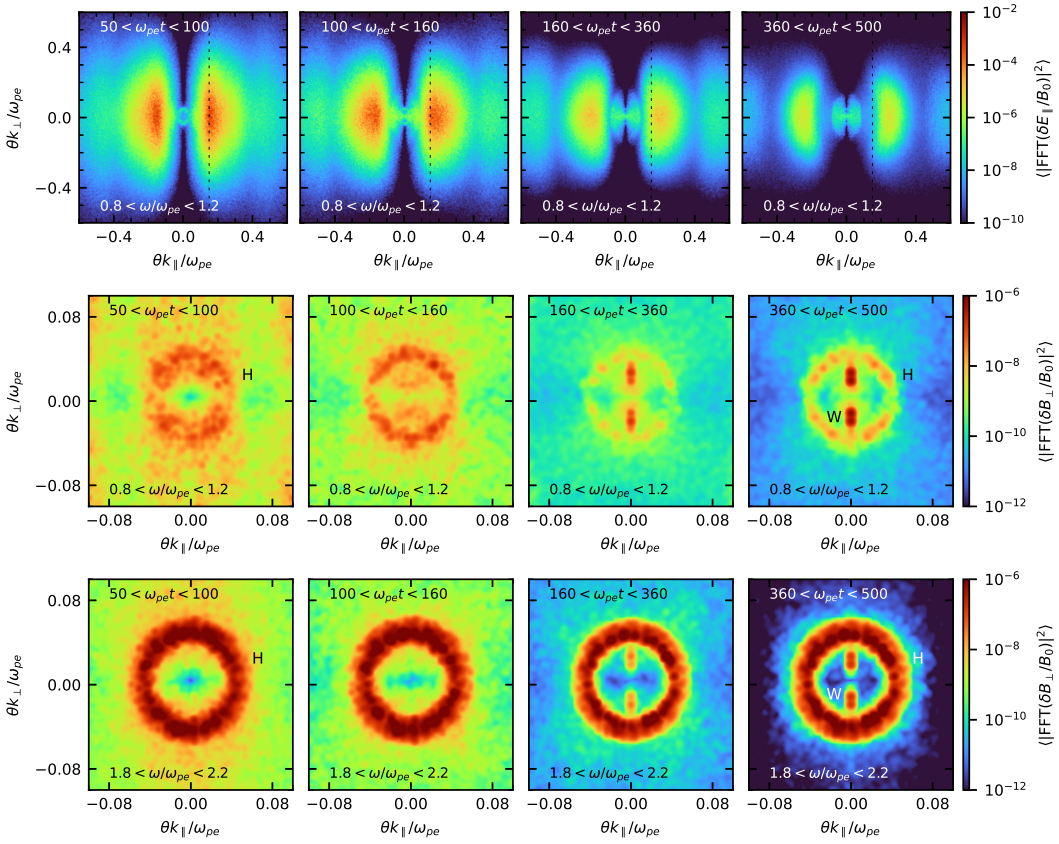

Figure 10. The same wave energy density spectra (normalized) as in Figure 9, but as functions of parallel and perpendicular wavenumbers (normalized), and averaged in the frequency intervals $0.8 < \omega/\omega_{pe} < 1.2$ (top and middle panels), and $1.8 < \omega/\omega_{pe} < 2.2$ (bottom panels).

direct coupling (or coalescence) of primary excitations, i.e., $L_+ + L_- \rightarrow 2T$, where here the symbol L is used generically, for two counterpropagating modes of either EB or LB nature. The resulting second harmonic (H$\rightarrow 2T$) is highly isotropic and very intense, in a broad frequency bandwidth centered on a predominantly downshifted frequency, i.e., $\omega \lesssim 2\omega_{pe}$. These properties strongly suggest that at the origin of radio emission the coalescence of primary excitations with downshifted frequencies also contributes. The frequency bandwidth of the second H radio emission is larger, about twice the bandwidth of the primary wave frequencies, as evidence that not only upshifted LB waves participate in the coalescence leading to the second H radio emission, but also the downshifted EB excitations. Thus, the maximum values of the radio frequencies are approximately given by the maximum (upshifted) frequencies of the primary excitations, $\omega_{2T,max} \simeq 2\omega_{LB,max} > 2\omega_{pe}$, while the minimum radio frequencies are given by the downshifted primary excitations, $\omega_{2T,min} \simeq 2\omega_{EB,min} < 2\omega_{pe}$.

In the later phases, i.e. $\omega_{pe}t > 160$, both primary excitations (forward and backward) decrease significantly in intensity but remain easy to identify because the spectra are less noisy. In the last two upper panels of Figures 9 and 10, their maxima have downshifted frequencies and move to higher wave numbers, typical for what we called ZB mode excitations. In Figures 9 and 10, lower panels, the H component of radio waves is produced with significant intensities and sufficiently isotropic spectra, mainly by the coalescence of the downshifted excitations, $ZB_+ + ZB_- \rightarrow 2T$. Their spectra are better outlined along

the dispersion curves of free EM modes, and the maxima in the frequency band drop below $2\omega_{pe}$. This is another important proof of the direct involvement of primary downshifted excitations in the generation of EM radio waves. It should be noted that excitations predominantly downshifted are signaled in this case much earlier ($\omega_{pe}t > 160$) than in case 2 ($\omega_{pe}t > 500$). The excitations of two counter-beams of electrons accelerate their relaxation and lead to the major involvement of the downshifted excitations in the generation of radio waves. The Weibel component (with high oblique propagation, $k_{\parallel} << k_{\perp}$) of the EM excitations also becomes more apparent in the subsequent phases ($\omega_{pe}t > 160$). We will return to it in a short comparative analysis in the next section.

In summary, our results are in agreement with previous studies (Henri et al., 2019; Sauer et al., 2019; Lazar et al., 2023a), demonstrating that the generation of radio emissions as escaping EM waves depends on the spectrum of the primary excitations, namely, their frequency and wavenumber, which in turn are conditioned by the properties of the electron beams. Two modes can be responsible for the downshifted excitations with direct but also indirect involvement in radio emission processes. In the early phase of our simulations, the EB modes are excited and can play both roles. When two counterpropagating electron beams trigger pairwise, forward and backward propagating EB excitations, these directly generate broad bands of the H component of radio waves, also downshifted from the (local) $2\omega_{pe}$. Instead, the EB excitations induced by a single (asymmetric) beam only contribute to the relaxation of the beam plasma distribution. The second mode responsible for downshifted excitations is represented by the ZB waves induced later by the relaxed distributions. Radio waves can be generated by coupling waves of the same type ZB in systems with two counterpropagating electron beams, or by the coalescence of ZB and secondary waves (resulting from wave-wave decays) in systems with a single electron beam.

3 Conclusions and discussions

Although downshifted ES waves have a well-established theoretical basis (Cairns, 1989; Gary, 1993; Willes & Cairns, 2000), and have also been observed in association with electron beams in the Earth's foreshock (Fuselier et al., 1985; Soucek et al., 2019), their involvement in the context of solar radio emissions has not yet been addressed. The most likely reason is that these excitations with lower frequencies, or downshifted with respect to the plasma frequency, do not conform to wave-wave interactions in the standard model of plasma radio emission (Melrose, 2008). Recent studies combining PIC simulations with rigorous predictions of wave dispersion and stability theory suggest, however, multiple implications of downshifted excitations in the generation of radio waves by electron beam plasmas (Sauer et al., 2019; Lazar et al., 2023a). We have therefore refined PIC simulations that prove the indirect or even direct involvement of downshifted primary excitations in the generation of radio emission in electron beam plasmas. Here we have analyzed in depth the primary excitations, while also accounting for the evolution of the electron beam at different time scales in radiative processes (Kasaba et al., 2001; Thurgood & Tsiklauri, 2015; Sauer et al., 2019). The main conclusions of our analysis can be sum up as follows.

When radio emissions are generated by the interaction of a single electron beam with the plasma, in particular, those satisfying condition (2), the downshifted excitations are identified in two distinct stages. For cases 1 and 2 (Table 1), the primary excitations from the early phases have frequencies close enough to the plasma frequency, the linear theory predicting ES instabilities of the electron-beam mode with frequency $\omega \lesssim \omega_{pe}$, still resonantly induced. Simulations show that their spectra, although narrowed around the plasma frequency, still include both downshifted and upshifted frequencies, respectively, the electron-beam (EB) and LB modes. Of which only the latter, i.e., LB excitations, are consistent with the plasma model driving EM (daughter) radio waves. However, the growing wave fluctuations act equally, whether they are upshifted or downshifted, on the electron beam, contributing to its plateau-on-tail or bump-on-tail relaxation. Such electron distributions are observed in situ in association with Langmuir fluctuations and radio emission (Ergun et al., 1998), and

simulations confirm that they are still at the origin of the radio emission. The distributions with flattened beams, more like gentle bumps-on-tail, also result from the relaxation of the systems that satisfy condition (1) (Kasaba et al., 2001; Lee et al., 2019). Moreover, their persistence over time could also provide a plausible solution to Sturrock's dilemma.

As a consequence of this relaxation, the spectrum of primary excitations also evolves towards higher wave numbers, on the LB branch with predominantly upshifted frequencies. Intense LB excitations are specific to beams with sufficiently low density, as in case 1, when they lead to bursty radiative processes, both in ES and EM spectra, and both with fundamental (F) and harmonic (H) components. In such situations, the wave conversion can be linear, e.g., LMC type, as well as (weakly) nonlinear in resonant wave-wave interactions. However, the involvement of downshifted primary excitations remains unclear, especially because of the noisy and even bursty spectra. For denser and/or cooler beams, the parametric excitations resulting from the wave-wave decay of the LB waves have lower intensities, but the spectra are less noisy, making it easier to distinguish the branch of the backscattered Langmuir (L_-) waves, the L_+ wave branch at very low wavenumbers (optical domain), and the low-frequency ion-sound waves $S_\pm$. Moreover, at larger time scales, the relaxed beams produce downshifted primary excitations, along the branch of the so-called Z-beam (ZB) mode. These ZB_+ waves can couple with L_- waves to explain the radio spectra obtained in this case, i.e., $ZB_+ + L_- \rightarrow 2T$, an H $= 2T$ emission more intense than the F component, also reported by the observations (Bakunin et al., 1990; Reiner & MacDowall, 2019). This mechanism appears to be sufficiently robust, as evidenced by the presence of the H component (albeit faint and obscured by other EM emission) until the end of our long-run simulations. Thus, we infer for the first time that the downshifted excitations can have not only an indirect action in the initial phases of beam relaxation but also a subsequent direct involvement in the generation of escaping radio waves.

This direct contribution of the downshifted excitations to radio emissions can be highlighted much earlier, and can be even more significant, as it emerges from the analysis of case 3, with two counter-beams of electrons, symmetric and with the same properties as in case 2. In case 3, a symmetric spectrum of downshifted primary excitations is obtained, in both forward and backward propagation directions. In the early stages, the ES excitations are again around the plasma frequency and include both downshifted EB and upshifted LB modes. However, by contrast to case 2, the intense counter-propagating waves couple and generate, on much shorter time scales, a broadband of the H component of radio waves, highly isotropic and also downshifted with respect to $2\omega_{pe}$. It results from the involvement of the downshifted primary excitations (with frequency $\omega < \omega_{pe}$) in the coalescence processes, e.g., $EB_- + EB_+ \rightarrow 2T(\omega < 2\omega_{pe})$. The energy conversion (from the kinetic energy of the electrons to ES and then EM waves) is significantly faster, and also contributes to the relaxation of the beams, reducing the time until only downshifted primary excitations are obtained. These are ZB excitations of lower intensity, this time symmetric and counterpropagating waves, which couple and generate the H radio emission, e.g., $ZB_+ + ZB_- \rightarrow 2T(\omega < 2\omega_{pe})$, still intense and highly isotropic.

The radiative mechanisms triggered by two counterbeams seem to be the most robust, but we should not ignore the Weibel (or filamentation) instabilities, which are also primary excitations, but of EM nature, i.e., the so-called EM electron beam modes. Karlický (2009) and Thurgood and Tsiklauri (2015) pointed out the competitiveness of these excitations, by taking over a significant part of the EM wave energy. For the same parameterization as in case 2 but in the absence of the uniform magnetic field (unmagnetized plasma), the simulations of Thurgood and Tsiklauri (2015) did not lead to radio emissions, while Lazar et al. (2023a) already found that the presence of the magnetic field has a favorable influence on the production of radio emissions. Our refined simulations (with the same $\omega_{pe}/|\Omega_e| = 100$) confirm this effect even for such dense electron beams. However, the background magnetic field does not have a direct influence on the ES excitations, but most likely, it inhibits other competing EM excitations, such as Weibel-like EM instabilities of the highly-

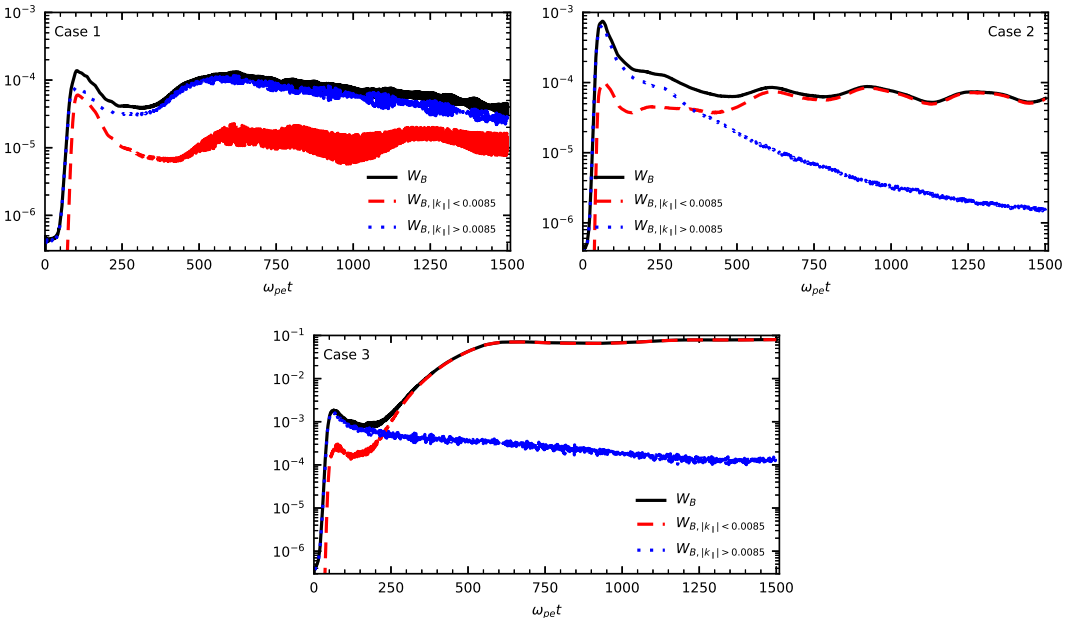

Figure 11. Partition of the wave magnetic energy density W_B (black), normalized to the initial kinetic energy of the beam, for cases 1, 2, and 3, between the highly oblique Weibel-like instability (dashed red) and the EM radio emission (blue dotted).

oblique (perpendicular) O-mode (Karlický, 2009; Lazar et al., 2010). Fig. 11 shows the total fluctuating magnetic energy density $W_B = \int dxdy\delta B_z^2/K_{b,0}$ (black), normalized to the initial kinetic energy density of the beam, $K_{b,0}$, for all our runs, case 1 (upper), 2 (middle) and 3 (lower). W_B is partitioned between the EM radio emission (blue dotted) and the perpendicular propagating mode (red dashed), most probably a Weibel-like excitation. In the initial phase ($\omega_{pe}t < 200$), the best conversion of the kinetic energy of the electrons into EM radio emissions occurs in case 3 with a little over 0.1 %; similarly, in case 2 with an efficiency slightly below 0.1 %, while in case 1, the efficiency is not much below 0.01 % and only slightly in favor of radio emissions. The radio spectra in case 2 have a peculiarity regarding the contrast between the F and H emissions, the latter being more intense. Moreover, this contrast increases in case 3 with two counterbeams of electrons, when the H emission becomes much more intense and the F component is almost absent. These characteristics can help identify certain radio plasma sources, in particular those with counterbeams of electrons with similar properties, i.e. (almost) symmetric counterbeams as those considered in case 3.

At larger time scales in Figure 11, the energy conversion remains favorable to radio emissions only in case 1, i.e, the blue-dotted curve remains always above the red-dashed, while in the other two cases the (relative) levels of radio emissions decrease, much steeper in case 2. However, in cases 2 and 3, the late efficiency of the Weibel excitations becomes very high, in case 3 reaching to convert almost 10 % of the initial kinetic energy of the electron beam. This is justified by the relaxation of the electron beam plasma to an anisotropic distribution with an effective temperature (or thermal spread) anisotropy still favorable to Weibel-type instabilities, but not to ES excitations at the origin of radio emissions. We can therefore expect that for weakly magnetized plasma systems, such as those considered here and specific to large heliocentric distances, e.g., at 1 AU and beyond, the spectra of radio emissions (especially the F component, see cases 1 and 2) may be obscured by Weibel-like excitations. Instead, the production of radio emissions, as well as the direct role of downshifted excitations can be significantly enhanced, both in the early and late phases, if

the magnetic fields are more intense, as, for instance, in sources of type II emission linked to shocks produced closer to the Sun, or in plasma sources of type III bursts from coronal flares. Recent PIC simulations confirm that in sufficiently strong magnetic fields the electron beam plasma interaction leads to an intense excitation in the field-aligned longitudinal mode, and to a significantly enhanced H emission, though the underlying wave-wave interactions in the magnetoactive plasma still remain to be elucidated (Lee et al., 2022).

To conclude, our analysis provides new arguments for the existence of extended regimes of electron beam plasmas (less debated so far), capable of producing radio emissions such as type II and type III solar radio bursts. Further investigation requires the relaxation of electron beams, in particular, the relaxed plateau-on-distributions that are still found to be effective in generating radio emissions. These radiative regimes can even involve reduced excitations, while their persistence in time has a particular relevance in solving Sturrock's dilemma. Such radio spectra dominated eventually by a (second) H radio emission have extended relevance in type III solar bursts (Reiner & MacDowall, 2019; Jebaraj et al., 2023). Another important conclusion is that the electron beams at the origin of the radio emissions do not necessarily have to have very low densities, as required in the standard plasma model for the excitation of primary Langmuir waves. Therefore, the present results motivate the upgrades of the standard model of radio plasma emission to include the new extended regimes of electron beams and downshifted primary excitations. This also has important implications in the remote diagnosis of radio plasma sources which, in general, is based on such a standard model.

Open Research Section

The simulation code we have used is adapted from the publicly available KEMPO1 code from Matsumoto and Omura (1993). The linear solutions used were obtained with the DIS-K code available at `https://github.com/ralopezh/dis-k` (R. López et al., 2021; R. A. López, 2023). The plots were produced with Matplotlib, available under the Matplotlib license at `https://matplotlib.org/`. The relevant input data are available at López (2024).

Acknowledgments
The authors acknowledge support from the Ruhr-University Bochum, the Katholieke Universiteit Leuven, and Qatar University. These results were also obtained in the framework of the projects C14/19/089 (C1 project Internal Funds KU Leuven), G0B5823N (FWO-Vlaanderen), WEAVE project G002523N / FI 706/31-1 (FWO-Vlaanderen / DFG-Germany), 4000134474 (SIDC Data Exploitation, ESA Prodex), Belspo project B2/191/P1/SWiM. Powered@NLHPC: This research was partially supported by the supercomputing infrastructure of the NLHPC (CCSS210001). The resources and services used in this work were provided by the VSC (Flemish Supercomputer Center), funded by the Research Foundation - Flanders (FWO) and the Flemish Government. The open access publication of this article was funded by Qatar National Library.

References

Bacchini, F., & Philippov, A. A. (2024, March). Fundamental, harmonic, and third-harmonic plasma emission from beam-plasma instabilities: a first-principles precursor for astrophysical radio bursts. *MNRAS*, *529*(1), 169-177. doi: 10.1093/mnras/stae521

Bakunin, L. M., Ledenev, V. G., Kosugi, T., & McLean, D. J. (1990, October). The harmonic structure of a type II burst on 12 May, 1983. *Solar Phys.*, *129*(2), 379-386. doi: 10.1007/BF00159048

Bale, S. D., Reiner, M. J., Bougeret, J. L., Kaiser, M. L., Krucker, S., Larson, D. E., &

Lin, R. P. (1999, June). The source region of an interplanetary type II radio burst. *Geophysical Research Letters*, *26*(11), 1573-1576. doi: 10.1029/1999GL900293

Baumgärtel, K. (2014). Ion dynamics in electron beam–plasma interaction: particle-in-cell simulations. *Annales Geophysicae*, *32*(8), 1025–1033. doi: 10.5194/angeo-32-1025-2014

Benson, R. F., Webb, P. A., Green, J. L., Carpenter, D. L., Sonwalkar, V. S., James, H. G., & Reinisch, B. W. (2006). Active Wave Experiments in Space Plasmas: The Z Mode. In J. W. Labelle & R. A. Treumann (Eds.), *Geospace electromagnetic waves and radiation* (Vol. 687, p. 3).

Boshuizen, C. R., Cairns, I. H., & Robinson, P. A. (2004, August). Electric field distributions for Langmuir waves in planetary foreshocks. *Journal of Geophysical Research (Space Physics)*, *109*(A8), A08101. doi: 10.1029/2004JA010408

Cairns, I. (2011). *The sun, the solar wind, and the heliosphere (iaga special sopron book series, vol. 4)*. Springer Berlin.

Cairns, I. H. (1989). Electrostatic wave generation above and below the plasma frequency by electron beams. *Physics of Fluids B: Plasma Physics*, *1*(1), 204-213. doi: 10.1063/1.859088

Cremades, H., Iglesias, F. A., St. Cyr, O. C., Xie, H., Kaiser, M. L., & Gopalswamy, N. (2015, September). Low-Frequency Type-II Radio Detections and Coronagraph Data Employed to Describe and Forecast the Propagation of 71 CMEs/Shocks. *Solar Phys.*, *290*(9), 2455-2478. doi: 10.1007/s11207-015-0776-y

Crosley, M. K., Osten, R. A., Broderick, J. W., Corbel, S., Eislöffel, J., Grießmeier, J.-M., ... Norman, C. (2016, oct). The search for signatures of transient mass loss in active stars. *The Astrophysical Journal*, *830*(1), 24. Retrieved from `https://dx.doi.org/10.3847/0004-637X/830/1/24` doi: 10.3847/0004-637X/830/1/24

Davis, I., Vedantham, H. K., Callingham, J. R., Shimwell, T. W., Vidotto, A. A., Zarka, P., ... Drabent, A. (2021, June). Large closed-field corona of WX Ursae Majoris evidenced from radio observations. *Astron. Astrophys.*, *650*, L20. doi: 10.1051/0004-6361/202140772

Dum, C. T. (1990a). Simulation studies of plasma waves in the electron foreshock: The transition from reactive to kinetic instability. *Journal of Geophysical Research: Space Physics*, *95*(A6), 8111-8122. Retrieved from `https://agupubs.onlinelibrary.wiley.com/doi/abs/10.1029/JA095iA06p08111` doi: 10.1029/JA095iA06p08111

Dum, C. T. (1990b). Simulation studies of plasma waves in the electron foreshock: The generation of downshifted oscillations. *Journal of Geophysical Research: Space Physics*, *95*(A6), 8123-8131. Retrieved from `https://agupubs.onlinelibrary.wiley.com/doi/abs/10.1029/JA095iA06p08123` doi: 10.1029/JA095iA06p08123

Ergun, R. E., Larson, D., Lin, R. P., McFadden, J. P., Carlson, C. W., Anderson, K. A., ... Bougeret, J.-L. (1998, aug). Wind spacecraft observations of solar impulsive electron events associated with solar type iii radio bursts. *The Astrophysical Journal*, *503*(1), 435. Retrieved from `https://dx.doi.org/10.1086/305954` doi: 10.1086/305954

Field, G. B. (1956, November). Radiation by Plasma Oscillations. *The Astrophysical Journal*, *124*, 555. doi: 10.1086/146261

Fuselier, S. A., Gurnett, D. A., & Fitzenreiter, R. J. (1985, May). The downshift of electron plasma oscillations in the electron foreshock region. *Journal of Geophysical Research*, *90*(A5), 3935-3946. doi: 10.1029/JA090iA05p03935

Gaelzer, R., Yoon, P. H., Ziebell, L. F., & Vinas, A. F. (2002, May). Dynamics of Electron Beam Propagation and Harmonic Langmuir Wave Generation. In *Agu spring meeting abstracts* (Vol. 2002, p. SH21D-05).

Ganse, U., Kilian, P., Spanier, F., & Vainio, R. (2012a, may). Nonlinear wave interactions as emission process of type II radio bursts. *APJ*, *751*(2), 145. Retrieved from `https://doi.org/10.1088/0004-637x/751/2/145` doi: 10.1088/0004-637x/751/2/145

Ganse, U., Kilian, P., Spanier, F., & Vainio, R. (2014, April). Fundamental and harmonic plasma emission in different plasma environments. *Astron. Astrophys.*, *564*, A15. doi: 10.1051/0004-6361/201322834

Ganse, U., Kilian, P., Vainio, R., & Spanier, F. (2012b, October). Emission of Type II Radio Bursts - Single-Beam Versus Two-Beam Scenario. *Solar Physics*, *280*(2), 551-560. doi: 10.1007/s11207-012-0077-7

Gary, S. P. (1993). *Theory of Space Plasma Microinstabilities*. Cambridge University Press, Cambridge. doi: 10.1017/CBO9780511551512

Henri, P., Sgattoni, A., Briand, C., Amiranoff, F., & Riconda, C. (2019). Electromagnetic simulations of solar radio emissions. *Journal of Geophysical Research: Space Physics*, *124*(3), 1475-1490. doi: 10.1029/2018JA025707

Jebaraj, I. C., Krasnoselskikh, V., Pulupa, M., Magdalenic, J., & Bale, S. D. (2023, sep). Fundamental–harmonic pairs of interplanetary type iii radio bursts. *The Astrophysical Journal Letters*, *955*(1), L20. Retrieved from `https://dx.doi.org/10.3847/2041-8213/acf857` doi: 10.3847/2041-8213/acf857

Karlický, M. (2009, January). Electron Beam-Plasma Interaction and the Return-Current Formation. *Astrophys. J.*, *690*(1), 189-197. doi: 10.1088/0004-637X/690/1/189

Kasaba, Y., Matsumoto, H., & Omura, Y. (2001, September). One- and two-dimensional simulations of electron beam instability: Generation of electrostatic and electromagnetic $2f_p$ waves. *Journal of Geophysical Research*, *106*(A9), 18693-18712. doi: 10.1029/2000JA000329

Kasaba, Y., Matsumoto, H., Omura, Y., Anderson, R. R., Mukai, T., Saito, Y., ... Kokubun, S. (2000, January). Statistical studies of plasma waves and backstreaming electrons in the terrestrial electron foreshock observed by Geotail. *J. Geophys. Res.*, *105*(A1), 79-104. doi: 10.1029/1999JA900408

Krafft, C., & Savoini, P. (2021, aug). Second harmonic electromagnetic emissions by an electron beam in solar wind plasmas with density fluctuations. *The Astrophysical Journal Letters*, *917*(2), L23. Retrieved from `https://dx.doi.org/10.3847/2041-8213/ac1795` doi: 10.3847/2041-8213/ac1795

Krafft, C., & Savoini, P. (2022, aug). Third and fourth harmonics of electromagnetic emissions by a weak beam in a solar wind plasma with random density fluctuations. *The Astrophysical Journal Letters*, *934*(2), L28. Retrieved from `https://dx.doi.org/10.3847/2041-8213/ac7f28` doi: 10.3847/2041-8213/ac7f28

Kuncic, Z., & Cairns, I. H. (2005, July). Planetary foreshock radio emissions. *Journal of Geophysical Research (Space Physics)*, *110*(A7), A07107. doi: 10.1029/2004JA010953

Lacombe, C., Harvey, C. C., Hoang, S., Mangeney, A., Steinberg, J. L., & Burgess, D. (1988, February). ISEE observations of radiation at twice the solar wind plasma frequency. *Annales Geophysicae*, *6*, 113-128.

Lazar, M., Dieckmann, M. E., & Poedts, S. (2010, February). Resonant Weibel instability in counterstreaming plasmas with temperature anisotropies. *Journal of Plasma Physics*, *76*(1), 49-56. doi: 10.1017/S0022377809008101

Lazar, M., López, R. A., Poedts, S., & Shaaban, S. M. (2023a). Kappa distributed electrons in solar outflows: beam-plasma instabilities and radio emissions. *Solar Physics*, *298*(5), 72. doi: 10.1007/s11207-023-02159-w

Lazar, M., López, R. A., Poedts, S., & Shaaban, S. M. (2023b, August). Instability of Langmuir-beam waves: Kappa-distributed electrons. *Physics of Plasmas*, *30*(8), 082106. doi: 10.1063/5.0159486

Lee, S.-Y., Yoon, P. H., Lee, E., & Tu, W. (2022, January). Simulation of Plasma Emission in Magnetized Plasmas. *The Astrophysical Journal*, *924*(1), 36. doi: 10.3847/1538-4357/ac32bb

Lee, S.-Y., Ziebell, L. F., Yoon, P. H., Gaelzer, R., & Lee, E. S. (2019, January). Particle-in-cell and Weak Turbulence Simulations of Plasma Emission. *The Astrophysical Journal*, *871*(1), 74. doi: 10.3847/1538-4357/aaf476

Li, B., & Cairns, I. H. (2013, jan). Type iii radio bursts in coronal plasmas with kappa particle distributions. *The Astrophysical Journal Letters*, *763*(2), L34. Retrieved from `https://dx.doi.org/10.1088/2041-8205/763/2/L34` doi: 10.1088/2041-8205/763/2/L34

Li, B., & Cairns, I. H. (2014, March). Fundamental Emission of Type III Bursts Produced

in Non-Maxwellian Coronal Plasmas with Kappa-Distributed Background Particles. *Solar Phys.*, *289*(3), 951-976. doi: 10.1007/s11207-013-0375-8

Lin, R. P., Potter, D. W., Gurnett, D. A., & Scarf, F. L. (1981, December). Energetic electrons and plasma waves associated with a solar type III radio burst. *The Astrophysical Journal*, *251*, 364-373. doi: 10.1086/159471

López, R. A. (2024). *Dataset for "Extended scenarios for solar radio emissions with downshifted electron beam plasma excitations [Dataset]".* Zenodo. Retrieved from `https://doi.org/10.5281/zenodo.14229977` doi: 10.5281/zenodo.14229977

López, R. A., Lazar, M., Shaaban, S. M., Poedts, S., & Moya, P. S. (2020, September). Alternative high-plasma beta regimes of electron heat-flux instabilities in the solar wind. *The Astrophysical Journal Letters*, *900*(2), L25. doi: 10.3847/2041-8213/abaf56

López, R., Shaaban, S., & Lazar, M. (2021). General dispersion properties of magnetized plasmas with drifting bi-Kappa distributions. DIS-K: Dispersion Solver for Kappa Plasmas. *Journal of Plasma Physics*, *87*(3), 905870310. doi: 10.1017/S0022377821000593

López, R. A. (2023, July). *ralopezh/dis-k: First public version [software].* Zenodo. Retrieved from `https://doi.org/10.5281/zenodo.8184896` doi: 10.5281/zenodo.8184896

Mann, G., Breitling, F., Vocks, C., Aurass, H., Steinmetz, M., Strassmeier, K. G., ... Zensus, J. A. (2018). Tracking of an electron beam through the solar corona with lofar. *A&A*, *611*, A57. Retrieved from `https://doi.org/10.1051/0004-6361/201629017` doi: 10.1051/0004-6361/201629017

Matsumoto, H., & Omura, Y. (Eds.). (1993). *Computer space plasma physics: Simulation techniques and software.* Terra Scientific Publishing Company, Tokyo.

Melrose, D. (2008). Coherent emission. *Proceedings of the International Astronomical Union*, *4*(S257), 305–315. doi: 10.1017/S1743921309029470

Melrose, D., McLean, D., & Labrum, N. (1985). *Solar radiophysics.* Cambridge Univ. Press Cambridge.

Menietti, J., Ye, S.-Y., Yoon, P., Santolik, O., Rymer, A., Gurnett, D., & Coates, A. (2009). Analysis of narrowband emission observed in the saturn magnetosphere. *Journal of Geophysical Research: Space Physics*, *114*(A6).

Nindos, A., Aurass, H., Klein, K. L., & Trottet, G. (2008, December). Radio Emission of Flares and Coronal Mass Ejections. Invited Review. *Solar Phys.*, *253*(1-2), 3. doi: 10.1007/s11207-008-9258-9

Onsager, T. G., & Holzworth, R. H. (1990). Measurement of the electron beam mode in earth's foreshock. *Journal of Geophysical Research: Space Physics*, *95*(A4), 4175-4186. doi: 10.1029/JA095iA04p04175

Pick, M., & Vilmer, N. (2008, October). Sixty-five years of solar radioastronomy: flares, coronal mass ejections and Sun Earth connection. *Astron. Astrophys. Rev.*, *16*, 1-153. doi: 10.1007/s00159-008-0013-x

Pierrard, V., & Lazar, M. (2010, November). Kappa Distributions: Theory and Applications in Space Plasmas. *Sol. Phys.*, *267*, 153-174. doi: 10.1007/s11207-010-9640-2

Pulupa, M., & Bale, S. D. (2008, apr). Structure on interplanetary shock fronts: Type ii radio burst source regions. *The Astrophysical Journal*, *676*(2), 1330. Retrieved from `https://dx.doi.org/10.1086/526405` doi: 10.1086/526405

Pulupa, M., Bale, S. D., Badman, S. T., Bonnell, J. W., Case, A. W., de Wit, T. D., ... Whittlesey, P. (2020, feb). Statistics and polarization of type iii radio bursts observed in the inner heliosphere. , *246*(2), 49. Retrieved from `https://dx.doi.org/10.3847/1538-4365/ab5dc0` doi: 10.3847/1538-4365/ab5dc0

Pulupa, M. P., Bale, S. D., & Kasper, J. C. (2010, April). Langmuir waves upstream of interplanetary shocks: Dependence on shock and plasma parameters. *Journal of Geophysical Research (Space Physics)*, *115*(A4), A04106. doi: 10.1029/2009JA014680

Raja, K. S., & Ramesh, R. (2013, sep). Low-frequency observations of transient quasi-periodic radio emission from the solar atmosphere. *The Astrophysical Journal*, *775*(1), 38. Retrieved from `https://dx.doi.org/10.1088/0004-637X/775/1/38` doi: 10.1088/0004-637X/775/1/38

Reid, H. A. S., & Ratcliffe, H. (2014, July). A review of solar type III radio bursts. *Research in Astronomy and Astrophysics*, *14*(7), 773-804. doi: 10.1088/1674-4527/14/7/003

Reiner, M. J., Kasaba, Y., Kaiser, M. L., Matsumoto, H., Nagano, I., & Bougeret, J. L. (1997, April). Terrestrial $2f_p$ radio source location determined from WIND/GEOTAIL triangulation. *Geophys. Res. Lett.*, *24*(8), 919-922. doi: 10.1029/97GL00472

Reiner, M. J., & MacDowall, R. J. (2019, July). New Evidence for Third Harmonic Electromagnetic Radiation in Interplanetary Type III Solar Radio Bursts. *Solar Phys.*, *294*(7), 91. doi: 10.1007/s11207-019-1476-9

Rhee, T., Ryu, C.-M., Woo, M., Kaang, H. H., Yi, S., & Yoon, P. H. (2009, mar). Multiple harmonic plasma emission. *The Astrophysical Journal*, *694*(1), 618. Retrieved from https://dx.doi.org/10.1088/0004-637X/694/1/618 doi: 10.1088/0004-637X/694/1/618

Sauer, K., Baumgärtel, K., Sydora, R., & Winterhalter, D. (2019, January). Parametric Decay of Beam-Generated Langmuir Waves and Three-Wave Interaction in Plateau Plasmas: Implications for Type III Radiation. *Journal of Geophysical Research (Space Physics)*, *124*(1), 68-89. doi: 10.1029/2018JA025887

Sauer, K., & Sydora, R. D. (2012, nov). Mode crossing effects at electron beam–plasma interaction and related phenomena. *Plasma Physics and Controlled Fusion*, *54*(12), 124045. Retrieved from https://dx.doi.org/10.1088/0741-3335/54/12/124045 doi: 10.1088/0741-3335/54/12/124045

Schleyer, F., Cairns, I. H., & Kim, E.-H. (2014). Linear mode conversion of langmuir/z mode waves to radiation: Averaged energy conversion efficiencies, polarization, and applications to earth's continuum radiation. *Journal of Geophysical Research: Space Physics*, *119*(5), 3392-3410. Retrieved from https://agupubs.onlinelibrary.wiley.com/doi/abs/10.1002/2013JA019364 doi: 10.1002/2013JA019364

Soucek, J., Píša, D., & Santolík, O. (2019). Direct measurement of low-energy electron foreshock beams. *Journal of Geophysical Research: Space Physics*, *124*(4), 2380-2392. doi: 10.1029/2019JA026470

Sturrock, P. (1964). Aas-nasa symposium on the physics of solar flares, ed. *WN Hess (NASA SP-50)*, *357*.

Swanson, D. G. (2003). *Plasma Waves, 2nd Edition*. doi: 10.1201/b15744

Thurgood, J. O., & Tsiklauri, D. (2015). Self-consistent particle-in-cell simulations of fundamental and harmonic plasma radio emission mechanisms. *Astronomy & Astrophysics*, *584*, A83. Retrieved from https://doi.org/10.1051/0004-6361/201527079 doi: 10.1051/0004-6361/201527079

Umeda, T. (2010). Electromagnetic plasma emission during beam-plasma interaction: Parametric decay versus induced scattering. *Journal of Geophysical Research: Space Physics*, *115*(A1). Retrieved from https://agupubs.onlinelibrary.wiley.com/doi/abs/10.1029/2009JA014643 doi: 10.1029/2009JA014643

Villadsen, J., & Hallinan, G. (2019, feb). Ultra-wideband detection of 22 coherent radio bursts on m dwarfs. *The Astrophysical Journal*, *871*(2), 214. Retrieved from https://dx.doi.org/10.3847/1538-4357/aaf88e doi: 10.3847/1538-4357/aaf88e

Volokitin, A. S., & Krafft, C. (2020, apr). Efficiency of electromagnetic emission by electrostatic turbulence in solar wind and coronal plasmas with density inhomogeneities. *The Astrophysical Journal Letters*, *893*(2), L47. Retrieved from https://dx.doi.org/10.3847/2041-8213/ab74de doi: 10.3847/2041-8213/ab74de

Warmuth, A., & Mann, G. (2005). The application of radio diagnostics to the study of the solar drivers of space weather. In K. Scherer, H. Fichtner, B. Heber, & U. Mall (Eds.), *Space weather: The physics behind a slogan* (pp. 49–68). Berlin, Heidelberg: Springer Berlin Heidelberg. Retrieved from https://doi.org/10.1007/978-3-540-31534-6_3 doi: 10.1007/978-3-540-31534-6_3

Willes, A. J., & Cairns, I. H. (2000). Generalized langmuir waves in magnetized kinetic plasmas. *Physics of Plasmas*, *7*(8), 3167-3180. doi: 10.1063/1.874180

Yoon, P. H., Gaelzer, R., Umeda, T., Omura, Y., & Matsumoto, H. (2003, February). Harmonic Langmuir waves. I. Nonlinear dispersion relation. *Physics of Plasmas*, *10*(2),

364-372. doi: 10.1063/1.1537238

Yoon, P. H., Weatherwax, A., Rosenberg, T., LaBelle, J., & Shepherd, S. (1998). Propagation of medium frequency (1–4 mhz) auroral radio waves to the ground via the z-mode radio window. *Journal of Geophysical Research: Space Physics*, *103*(A12), 29267–29275. doi: 10.1029/1998JA900032

Ziebell, L. F., Petruzzellis, L. T., Yoon, P. H., Gaelzer, R., & Pavan, J. (2016, feb). Plasma emission by counter-streaming electron beams. *The Astrophysical Journal*, *818*(1), 61. doi: 10.3847/0004-637X/818/1/61

Ziebell, L. F., Yoon, P. H., Gaelzer, R., & Pavan, J. (2014, November). Plasma Emission by Weak Turbulence Processes. *The Astrophysical Journal Letters*, *795*(2), L32. doi: 10.1088/2041-8205/795/2/L32